EXACT ANALYSIS OF UNSTEADY CONVECTIVE DIFFUSION ON SYNOVIAL FLUID WITH COMBINED EFFECTS OF MAGNETIC AND ELECTRIC FIELDS

R. VijayaKumar,[1] M. Seenivasan,[2,*] S. Senthamilselvi, [3] & T.S. Suchita,[3]

[1]Mathematics Section, FEAT, Annamalai University, Annamalai Nagar, Tamil Nadu, India

Deputed to Department of Mathematics, Periyar Government Arts College, Tamil Nadu, India.

[2]Department of Mathematics – CDOE, Annamalai University, Annamalai Nagar, Chidambaram, Tamil Nadu, India

[3]Department of Mathematics, Vels Institute of Science, Technology & Advanced Studies, Tamil Nadu, India

*Address all correspondence to: M. Seenivasan, Department of Mathematics – CDOE, Annamalai University, Annamalai Nagar, Chidambaram, Tamil Nadu, India, E-mail: emseeni@yahoo.com

ABSTRACT: A mathematical model describing to study the impact of electromagnetic fields on human joint cartilaginous cells and the nutrients that go from synovial fluid to the cartilage are examined in this study. With dimensionless time, the dispersion coefficient rises. It makes to understand how much nutrition is transported to the synovial joint. Compared to high-molecular-weight solutes, low-molecular-weight solutes have a lesser concentration distribution at the same depth in articular cartilage. Therefore, for low-molecular-weight solutes, nutrition transport is dominated by diffusion, while for high-molecular-weight solutes, nutrition transport is dominated by a mechanical pumping action. It also predicts that the concentration in the articular cartilage would decrease as the electric field, Hartmann number, and rheological parameter rise. This might have adverse effects since the cartilage cells will get less nutrition. For various parameters, including the electric field, Hartmann number, porosity parameter, and rheological

parameter of gel formation, the dispersion coefficient and mean concentration have been calculated and graphically shown.

KEY WORDS: generalized dispersion model, electromagnetic fields, and Bingham fluid

1. INTRODUCTION

1.1 Motivation for Mathematical Modeling

The inclusion of a comprehensive mathematical framework in this study is deliberate and necessary. Modeling the synovial fluid, a complex biological fluid with non-Newtonian characteristics, requires the use of the Bingham fluid model to adequately capture its viscoplastic behavior. Furthermore, the incorporation of electromagnetic fields and porous boundaries introduces additional nonlinearities that cannot be approximated with simpler formulations. The long-form mathematical presentation is essential for providing exact solutions and deriving expressions for key biomedical indicators such as dispersion coefficients and mean solute concentration. These solutions offer analytical clarity and facilitate parametric sensitivity studies that are otherwise challenging with purely numerical approaches.

1.2 Medical and Biological Context

The human synovial joint is a biomechanically and biochemically active environment. Synovial fluid plays a pivotal role in transporting nutrients such as glucose and amino acids to the avascular articular cartilage. Disruptions in this transport mechanism, especially due to altered rheological properties or external electromagnetic interventions, can impact cartilage health and potentially accelerate degenerative joint diseases. This study models the influence of electric and magnetic fields on this transport process, a topic of direct relevance in designing bio-compatible prosthetics and minimizing haemolysis a phenomenon where red blood cells rupture due to mechanical or electrical stress, releasing hemoglobin.

1.3 Mathematical and Biomathematical Significance

From a biomathematics perspective, the presented model is well-posed under physiological boundary conditions, including Beavers–Joseph slip conditions at the porous cartilage surface. The model builds upon and extends classical dispersion theories such as those by Taylor (1953), Gill and Sankarasubramanian (1970) to a more physiologically relevant setting. The mathematical structure ensures boundedness and physical realism of the solution, especially in the long-time behavior of solute concentration and dispersion. Moreover, this formulation offers insight into how varying physical and biomedical parameters (e.g., Hartmann number, porosity, rheological coefficients) influence nutrient transport and fluid mechanics in joint tissues. Such insights are critical not only for theoretical advancement but also for informing experimental and clinical practices. A detailed interpretation of the results, bridging the analytical findings with biomedical implications, has been added in the discussion section. The current model thus represents an integrative approach merging exact mathematical analysis with applied medical relevance—that strengthens the study's contribution to both computational biology and biomedical engineering. Interest in fluid dynamical research has grown as a result of recent advancements on several aspects of dispersion in blood flow. Significant biological applications of solute dispersion in non-Newtonian fluid flow, such as the investigation of passive impurity dispersion in artery blood flow, extend beyond mass transfer in polymer solutions. Blood is known to behave in a non-Newtonian manner, especially when it passes through a system at low shear rates. In addition to being of physiological significance in synovial joints, Coronary Artery Disease (CAD), and the trachea (wind pipe), the study of couple stress fluid dispersion in microchannels surrounded by porous medium is of significance to many companies, especially the chemical industry. It is also of importance in atmospheric pollution in the dispersion of aerosols Rudraiah et al. (2011). Experimental studies have demonstrated that the characteristics of blood flow vary depending on the location of the body by Christopherson and Dowson (1959). Depending on the issues being studied, this calls for taking into account various fluids in various physiological contexts. In order to better understand the haemolysis brought on by metal artificial organs in biomedical engineering, we investigate an unstable dispersion in a fluid that is poorly conducting in the presence of a transverse electric field and magnetic field in this research. Many types of blood injury are currently caused by metal-made artificial organs. Haemolysis, or the loss of haemoglobin from erythrocytes (RBC) in the blood, is one of the most significant types of blood damage. There are three possible causes of haemolysis: mechanical, chemical, and physiological.

In this study, we focus on haemolysis brought on by mechanical processes since metal-based prosthetic organs are not biocompatible with natural organs such as synovial cartilages. Either large shear stresses or mild stresses are produced by the metal organs, and these stresses ultimately result in a force. The RBCs in arteries are driven to a specific area by this force. A condition known as haemolysis will occur when the buildup of red blood cells bursts, releasing haemoglobin. We must select the right material to create prosthetic organs that won't result in high or low stress levels in order to defeat this illness. In order to regulate haemolysis, we suggest in this study using a transverse electric field, the stress nature of synovial fluid that is weakly conducting, and slide at the porous surface of cartilage. Artificial cartilages function similarly to genuine cartilages because of the slip and pair stress, which make their surfaces resemble those of natural tissues. Both high and low shear stresses are generated by the metal organs, and these stresses ultimately result in a force. The arteries red blood cells are driven to a specific area by this force. This condition is known as haemolysis. The buildup of red blood cells will break, releasing haemoglobin. Selecting the right material to create prosthetic organs that won't result in high or low stress levels is essential to overcoming this illness.

Mallika and Rudraiah (2011) investigated the unsteady convective diffusion of RBCs in the physiological fluid modeled as couple stress fluid, using the Generalized Dispersion model of Gill and Sankarasubramanian (1970). Nirmala P.Ratchagar and VijayaKumar (2014) utilised the generalised dispersion model of Gill and Sankarasubramanian (1970) and Taylor (1953), which is a specific instance of the generalised dispersion model for asymptotic values of time, investigated the impact of coupling stress and magnetic field on the unsteady connective diffusion of erythrocytes in the plasma flow. This means that the generalised dispersion model asymptotically reduces to Taylor's dispersion model. Das et al. (2021) exploited the immersed boundary technique with staggered grids to examine the impact of wall absorption on dispersion. Research on the analysis of drug diffusion in arterial blood, control release, and at the targeted sites is crucial in the field of biomedical engineering by Shaw et al. (2014), Das et al. (2021), Beg and Roy (2022), Le and Tran (2022), Mohseni and Domfeh (2023). Injection of solute (drug) at regular intervals is also an essential field of study. A number of academics have, nonetheless, focused on the drug delivery mechanism and made contributions using various techniques. Jyoti et al. (2023) performed how a chemically reactive solute will disperse across mobile to immobile phase when injected into the fluid flowing within a long circular tube. Rushi Kumar et al.(2024) examined the nutritional transport of generalised dispersion under the influence of an electric and magnetic field in order to study the model for the synovial fluid, also referred to as joint fluid and found in the knee joints. The generalised dispersion model and perturbation approach were used to investigate the synovial fluid behaviour. The effects of magnetic and electric fields on solute transport have become increasingly relevant. For instance, Nihaal Kandavkovi Mallikarjuna et al. (2025) presents detailed analysis of magneto-electro-hydrodynamic (MEHD) flows in complex geometries, confirming that electromagnetic forces significantly alter flow profiles and dispersion characteristics.

The goal of this work has been to examine the flow properties of a Bingham plastic fluid through a porous material when both an electric and magnetic field are present. In order to emphasise the dispersion coefficient and mean concentration, the generalised dispersion model of Sankarasubramanian and Gill (1970) has been applied. The study validates its results by comparing with earlier couple stress models and shows that differences in results arise due to the distinct rheological nature of the Bingham fluid. This comparative approach underlines the added value and necessity of the Bingham model for certain biomedical applications.

2. MATHEMATICAL AND BIOMATHEMATICAL SIGNIFICANCE

The constitutive equation for blood, expressed as Bingham fluid, is as follows, according to Misra and Adhikary (2017)

$$\tau_{xy} = -\mu_0 \frac{\partial u_f^*}{\partial y} \pm \tau_0 \qquad if \qquad \left|\tau_{xy}\right| > \tau_0 \tag{1}$$

$$\frac{\partial u_f^*}{\partial y} = 0 \qquad if \qquad \left|\tau_{xy}\right| < \tau_0 \tag{2}$$

In the channel, equations (1) and (2) depict the two stages of blood flow. The flat velocity profile in the central core region creates the plug flow region. Shear stress in this plug flow zone is less than yield stress τ_0.

The governing equations and associated boundary conditions are derived under the following presumptions: Steady laminar and fully developed flow (unidirectional) in a channel bounded by porous layers and separated by a distance 2h. An electric field and a uniform magnetic field B_0 are supplied to the blood flow in the y-direction. The physical structure of the human knee joint is depicted in FIG.1, Tandon et al.(1988), Alshehri and Sharma (2017). In a channel enclosed by porous beds, the solute diffuses over the porous medium in a fully formed flow. For concentration C, which depends on coordinates x' and y and time (t), a slug is added. Under the aforementioned presumption, the following governing equations apply to the incompressible flow of a non-Newtonian fluid in cartesian coordinates:

Region 1:

$$\frac{\partial u_f^*}{\partial x'} = 0 \tag{3}$$

$$-\frac{\partial p'}{\partial x'} + \mu \frac{\partial \tau_{xy}}{\partial y} - \frac{\mu}{k} u_f^* - B_0^2 \sigma_0 u_f^* + \rho_e E_x = 0 \tag{4}$$

$$-\frac{\partial p'}{\partial y} + \rho_e E_y = 0 \tag{5}$$

The concentration C satisfying the convective diffusion equation gives

$$\frac{\partial C}{\partial t} + u_f^* \frac{\partial C}{\partial x'} = D\left(\frac{\partial^2 C}{\partial x'^2} + \frac{\partial^2 C}{\partial y^2}\right) \tag{6}$$

Region 2:

$$\frac{\partial u_p^*}{\partial x} = 0 \tag{7}$$

$$-\frac{\partial p'}{\partial x'} - \frac{\mu}{k} u_p^* + -B_0^2 \sigma_0 u_p^* + \rho_e E_x + \alpha_0 = 0 \tag{8}$$

$$-\frac{\partial p'}{\partial y} + \rho_e E_y = 0 \tag{9}$$

Boundary conditions for concentration and velocity are

$$\frac{\partial u_f^*}{\partial y} = -\frac{\alpha}{\sqrt{k}} (u_f^* - u_p^*) \qquad at \qquad y = h \tag{10}$$

$$\frac{\partial u_f^*}{\partial y} = \frac{\alpha}{\sqrt{k}} (u_f^* - u_p^*) \qquad at \qquad y = -h \tag{11}$$

The symmetric conditions,

$$\frac{\partial u_f^*}{\partial y}=0 \qquad at \qquad y=0 \tag{12}$$

$$u_f^* = u_{pf}^* \qquad at \qquad y=y_c \tag{13}$$

The initial and boundary conditions on concentration.

$$C(0,x',y)=\begin{cases} C_0, |x'| \le \frac{X'_s}{2} \\ 0, |x'| > \frac{X'_s}{2} \end{cases} \tag{14}$$

$$\frac{\partial C(t,x',0)}{\partial y}=\frac{\partial C(t,x',h)}{\partial y}=0 \tag{15}$$

$$C(t,\infty,y)=\frac{\partial C(t,\infty,y)}{\partial x'}=0 \tag{16}$$

where, u_f^* is the component of velocity, p^* is the pressure, μ is the viscosity of the fluid, B_0 is the applied magnetic field, σ_0 is the electrical conductivity, E_i is the electric field, ρ_e is the density, t is the time, D is the molecular diffusivity, k is the permeability of the porous medium, u_p^* is the Darcy velocity, α is the slip parameter, $C_0^{'}$ is the reference concentration, τ_{xy} is the shear stress, μ_0 is the plastic dynamic viscosity, $\alpha_0=\frac{\beta_1\tau_0}{\sqrt{k}}$ β_1 is experimentally determined constant, u_f is the axial velocity, τ_0 is the yield stress, C_0 is the initial concentration of the initial slug input of length X_s. Beavers and Joseph's (1967) slip condition at the lower and upper permeable surfaces is represented by equations (10) and (11).

Introducing the non-dimensional quantities

$$U_f=\frac{u_f^*}{u'}, u_p=\frac{u_p^*}{u'}, \eta=\frac{y}{h}, X'=\frac{x'}{h\,Pe}, X_s=\frac{x'_s}{h\,Pe}, \ p^*=\frac{p}{\rho u'^2}, \tau=\frac{Dt}{h^2}, \theta=\frac{C}{C_0}, \rho_e=\frac{\hat{\rho}_0\ h^2}{\epsilon_0\ V}, E_x^*=\frac{E_x h}{V}$$

In non-dimensional form, equations (4) to (6) are

Region 1:

$$\frac{d^4 U_f}{\partial \eta^4} - M^2 U_f = s_2 + We\, s_1 (1 - \alpha_c \eta) \tag{17}$$

$$\frac{\partial \theta}{\partial \tau} + U \frac{\partial \theta}{\partial X'} = \frac{1}{Pe^2}\left(\frac{\partial^2 \theta}{\partial X'^2} + \frac{\partial^2 \theta}{\partial \eta^2}\right) \tag{18}$$

we define the axial coordinate moving with the average velocity of flow as $\xi = x' - \tau \bar{u}$ which is in dimensionless form $\xi = X' - \tau$,.

Then equation (18) becomes

$$\frac{\partial \theta}{\partial \tau} + U_f \frac{\partial \theta}{\partial \xi} = \frac{1}{Pe^2}\left(\frac{\partial^2 \theta}{\partial \xi^2} + \frac{\partial^2 \theta}{\partial \eta^2}\right) \tag{19}$$

where, $U_f = \dfrac{U_f - \bar{U}_f}{\bar{U}_f}$

We= electric number

Region 2:

$$U_p = -\frac{\left[\dfrac{\mathrm{Re}}{Pe} + We\, s_1 (1 - \alpha_c \eta)\right]}{\sigma^2 + M^2} \tag{20}$$

The dimensionless form of the initial and boundary conditions (10) to (16)

$$\frac{\partial U_f}{\partial \eta} = -\alpha\sigma (U_f - U_p) \qquad at \qquad \eta = 1 \tag{21}$$

$$\frac{\partial U_f}{\partial \eta} = \alpha\sigma (U_f - U_p) \qquad at \qquad \eta = -1 \tag{22}$$

$$\frac{\partial U_f}{\partial \eta} = 0 \qquad at \qquad \eta = 0 \tag{23}$$

$$U_f = U_{pf} \qquad at \qquad \eta = \eta_c \tag{24}$$

$$\left.\begin{aligned}
&\theta(0,\xi,\eta)=\begin{cases}1, |\xi|\le \frac{\xi_s}{2}\\ 0, |\xi|>\frac{\xi_s}{2}\end{cases}\\
&\frac{\partial\theta(\tau,\xi,0)}{\partial\eta}=\frac{\partial\theta(\tau,\xi,1)}{\partial\eta}=0\\
&\theta(\tau,\infty,\eta)=\frac{\partial\theta(\tau,\infty,\eta)}{\partial\xi}=0
\end{aligned}\right\} \tag{25}$$

Where $M^2=\frac{\sigma_0 B_0^2 h^2}{\mu_0}$ is the Hartmann, $\sigma=\frac{h}{\sqrt{k}}$ is the porous parameters, $We=\frac{\varepsilon_0 V^2}{\mu_0}$ is the electric numbers , $\mathrm{Re}=\frac{\rho u' h}{\mu_0}$ is the Reynolds number, $Pe=\frac{u' h}{D}$ is the Peclet number,

3. METHOD OF SOLUTION

3.1 Velocity Distribution

The solution of equation (15) subject to (17) can be written as

$$U_f=\begin{cases}A_1 e^{M\eta_c}+A_2 e^{-M\eta_c}-\frac{1}{M^2}We\ \ s_1(1-\alpha_c\eta_c),\ if\ \ 0<\eta\le\eta_c\\ A_1 e^{M\eta}+A_2 e^{-M\eta}-\frac{1}{M^2}We\ \ s_1(1-\alpha_c\eta),\ if\ \ \eta_c<\eta\le 1\end{cases} \tag{26}$$

where A_1, A_2, and s_1 are constants given in Appendix 1.

The axial velocity components that have been normalised are

$$U_f'=\frac{U_f-\bar{U}_f}{\bar{U}_f} \tag{27}$$

where

$$\begin{aligned}\bar{U}_f=\int_0^1 U_f(\eta)d\eta=\eta_C\left(A_1 e^{M\eta_c}+A_2 e^{-M\eta_c}-\frac{1}{M^2}We\ \ s_1(1-\alpha_c\eta_c)\right)+\frac{1}{2M}\{\left(A_2(2e^{-M}-2e^{-M\eta_c})\right)-2A_1(2e^{M}-e^{M\eta_c})\\
+s_1 We(-1+\eta_c)(-2+\alpha_c+\alpha_c\eta_c)\}\end{aligned} \tag{28}$$

The generalised dispersion model of Gill and Sankarasubramanian (1970), which is expressed as a series expansion in the form of

$$\theta(\tau,\xi,\eta)=\theta_m(\tau,\xi)+f_1(\tau,\eta)\frac{\partial\theta_m}{\partial\xi}+f_2(\tau,\eta)\frac{\partial^2\theta_m}{\partial\xi^2}+... \tag{29}$$

where, θ_m is the dimensionless cross sectional average concentration, given by

$$\theta(\tau,\xi)=\int_0^1\theta(\tau,\xi,\eta)d\eta \tag{30}$$

Integrating equation (19) with respect to η in (0, 1) and using the equation (29) and (30), we get

$$\frac{\partial\theta_m}{\partial\tau}=\frac{1}{Pe^2}\frac{\partial^2\theta_m}{\partial\xi^2}-\frac{\partial}{\partial\xi}\int_0^1 U_f^{'}\left(\theta_m(\tau,\xi)+f_1(\tau,\eta)\frac{\partial\theta_m}{\partial\xi}+f_2(\tau,\eta)\frac{\partial^2\theta_m}{\partial\xi^2}+...\right)d\eta \tag{33}$$

In this model we write

$$\frac{\partial\theta_m}{\partial\tau}=\sum_{i=1}^{\infty}K_i(\tau)\frac{\partial^i\theta}{\partial\xi^i} \tag{34}$$

Comparing (33) and (34) we get $K_i(\tau)$

$$K_i(\tau)=\frac{\delta_{ij}}{Pe^2}-\int_0^1 U_f^{'}\,f_{i-1}(\tau,\eta)\,d\eta \qquad (i=1,2,3,....\ and\ \ j=2) \tag{35}$$

where, $f_{-1}=0$, δ_{ij} is the Kroneckar delta defined by

$$\delta_{ij}=\begin{cases}1, if\ i=j\\ 0, if\ i\neq j\end{cases}$$

Substituting equation (29) in (19), using this model we write

$$\frac{\partial^{k+1}\theta_m}{\partial\tau\,\partial\xi^k}=\sum_{i=1}^{\infty}K_i(\tau)\frac{\partial^{k+i}\theta_m}{\partial\xi^{k+i}} \qquad \text{for k=1,2,3,…}$$

we obtain

$$\left(\frac{\partial f_1}{\partial \tau}-\frac{\partial^2 f_1}{\partial \eta^2}+U_f^{'}+K_1(\tau)\right)\frac{\partial \theta_m}{\partial \xi}$$
$$+\left(\frac{\partial f_2}{\partial \tau}-\frac{\partial^2 f_2}{\partial \eta^2}+U_f^{'}f_1+K_1(\tau)f_1+K_2(\tau)-\frac{1}{Pe^2}\right)\frac{\partial^2 \theta_m}{\partial \xi^2} \qquad 36$$
$$+\sum_{k=1}^{\infty}\left(\frac{\partial f_{k+2}}{\partial \tau}-\frac{\partial^2 f_{k+2}}{\partial \eta^2}+U_f^{'}f_{k+1}+K_1(\tau)f_{k+1}+\left(K_2(\tau)-\frac{1}{Pe^2}\right)f_k+\sum_{i=3}^{k+2}K_i f_{k+2-i}\right)\frac{\partial^{k+2}\theta_m}{\partial \xi^{k+2}}=0$$

with $f_0 = 1$. Equating the coefficients of $\frac{\partial^k \theta_m}{\partial \xi^k}$ (k=1,2,3,…) in equation (36) to zero, we obtain the following set of partial differential equations:

$$\frac{\partial f_1}{\partial \tau}=\frac{\partial^2 f_1}{\partial \eta^2}-U_f^{'}-K_1(\tau) \qquad (37)$$

$$\frac{\partial f_2}{\partial \tau}=\frac{\partial^2 f_2}{\partial \eta^2}-U_f^{'}f_1-K_1(\tau)f_1-K_2(\tau)+\frac{1}{Pe^2} \qquad (38)$$

$$\frac{\partial f_{k+2}}{\partial \tau}=\frac{\partial^2 f_{k+2}}{\partial \eta^2}-U_f^{'}f_{k+1}-K_1(\tau)f_{k+1}-\left(K_2(\tau)-\frac{1}{Pe^2}\right)f_k-\sum_{i=3}^{k+2}K_i f_{k+2-i} \qquad (39)$$

To find K_i's we know the f_k's and its corresponding initial and boundary conditions are

$$\frac{\partial f_k(\tau,0)}{\partial \tau}=0 \qquad (40)$$

$$\frac{\partial f_k(\tau,1)}{\partial \tau}=0 \qquad (41)$$

$$\int_0^1 f_k(\tau,\eta)d\eta=0 \qquad \text{for k=1,2,3,…} \qquad (42)$$

for k=1,2,3,…

From equation (35) for i=1, using f_0=1, we get K_1 as

$$K_1(\tau)=0 \qquad (43)$$

From equation (35), we get,

$$K_2(\tau) = \frac{1}{Pe^2} - \int_0^1 U'_f f_1 \, d\eta \qquad (44)$$

To Evaluate $K_2(\tau)$

let $f_1 = f_{10}(\eta) + f_{11}(\tau,\eta)$ (45)

where, $f_{10}(\eta)$ corresponds to an infinitely wide slug which is independent of τ and f_{11} is τ dependent satisfying

$$\frac{\partial f_{10}(\eta)}{\partial \eta} = 0 \ \ at \ \eta = 0,1 \qquad (46)$$

$$\int_0^1 f_{10}(\eta) d\eta = 0 \qquad (47)$$

Using the (46) and (47) in (38) implies

$$\frac{\partial^2 f_{10}(\eta)}{\partial \eta^2} = \begin{cases} s_7, & 0 < \eta \le \eta_c \\ A_1 e^{M\eta} + A_2 e^{-M\eta} - \frac{We\, s_1}{M^2}(1 - \alpha_c \eta), & \eta_c < \eta \le 1 \end{cases} \qquad (48)$$

$$\frac{\partial f_{10}}{\partial \eta} = \frac{\partial f_{11}}{\partial \eta} \qquad (49)$$

Solving the equation (49) with conditions (46) and (47) is

$$f_{10}(\eta) = \begin{cases} \frac{s_7}{2}\left(\eta^2 + \frac{1}{3}\right), & 0 < \eta \le \eta_c \\ A_1 \frac{e^{M\eta}}{M^2} + A_2 \frac{e^{-M\eta}}{M^2} - \frac{We\, s_1}{M^2}\left(\frac{\eta^2}{2} - \alpha_c \frac{\eta^3}{6}\right) + A_5 \eta + A_6, & \eta_c < \eta \le 1 \end{cases} \qquad (50)$$

Equation (49) is heat conduction type and its solution satisfying condition $f_{11}(\tau,\eta) = -f_{10}(\eta)$

of the form

$$f_{11} = \sum_{n=1}^{\infty} B_n e^{-\lambda_n^2 \tau} Cos \lambda_n \eta \qquad (51)$$

where, $B_n = -2\int_0^1 f_{10}(\eta) Cos(\lambda_n \eta) d\eta$ (52)

and $\lambda_n = n\pi$. Substituting (50) in (52) we get,

$$B_n = \frac{-s_7(6n\pi\eta_c Cos(n\pi\eta_c) + (-6 + n^2\pi^2(1+3\eta_c^2))Sin(n\pi\eta_c))}{3n^2\pi^2}$$
$$-2(\frac{-A_6 Sin(n\pi\eta_c)}{n\pi} - \frac{A_5(-Cos(n\pi) + Cos(n\pi\eta_c) + n\pi\eta_c Sin(n\pi\eta_c))}{n^2\pi^2}$$
$$+\frac{1}{6M^2n^4\pi^4} s_1 We\alpha_c(3(-2+n^2\pi^2)Cos(n\pi) + (6-3n^2\pi^2\eta_c^2)Cos(n\pi\eta_c)$$
$$+n\pi\eta_c(6-n^2\pi^2\eta_c^2)Sin(n\pi\eta_c)) +$$
$$\frac{1}{2M^2n^3\pi^3} s_1 We(-2n\pi\, Cos(n\pi) + 2n\pi\eta_c Cos(n\pi\eta_c) + (-2+n^2\pi^2\eta_c^2)Sin(n\pi\eta_c)) +$$
$$\frac{1}{M^2(M^2+n^2\pi^2)} A_2 e^{-M(1+\eta_c)}(-e^{-M\eta_c} M\, Cos(n\pi) + e^M (M\, Cos(n\pi\eta_c) - n\pi\, Sin(n\pi\eta_c)) +$$
$$\frac{1}{M^4 + M^2n^2\pi^2} A_1(e^M M\, Cos(n\pi) - e^{M\eta_c}(M\, Cos(n\pi\eta_c) + n\pi\, Sin(n\pi\eta_c)))$$

Substituting the values of $f_{11}(\eta)$ and $f_{10}(\eta)$ in (46) we get f_1 as

$$f_1(\tau,\eta) = f_{11}(\eta) - 2\sum_{n=1}^{\infty} B_n e^{-\lambda_n^2\tau} Cos\lambda_n\eta \int_0^1 f_{10}(\eta) Cos(\lambda_n\eta) d\eta \quad (53)$$

Substituting (53) into (44) we get we get solution of dispersion coefficient with help of MATHEMATICA 12.0.

$$K_2(\tau) = \frac{1}{Pe^2} - \int_0^1 U_f^{'} f_1\, d\eta$$

where,s_1, s_2, s_3, s_4, s_5, s_6, A_1, A_2, A_3, A_4, A_5, and A_6 are the constants, given in the Appendix.

Similarly, and so on are obtained and we found that$K_i(\tau)$, i>2 are negligibly small compared to $K_2(\tau)$. Hence the dispersion model (34) now leads to

$$\frac{\partial\theta_m}{\partial\tau} = K_2 \frac{\partial^2\theta_m}{\partial\xi^2} \quad (54)$$

The exact solution of (54) satisfying the condition (25) can be obtained using Fourier Transform by Sankar Rao (1995) as

$$\theta_m(\xi,\tau)=\frac{1}{2}\left(erf\left(\frac{\frac{\xi_s}{2}+\xi}{2\sqrt{T}}\right)+erf\left(\frac{\frac{\xi_s}{2}-\xi}{2\sqrt{T}}\right)\right)$$

where, $T=\int_0^{\tau}K_2(\eta)d\eta$ and $erf(\xi)=\frac{2}{\sqrt{\pi}}\int_0^{\xi}e^{-z^2}dz$

4. RESULT AND DISCUSSIONS

As demonstrated in the work of Nirmala Ratchagar and Vijayakumar (2014), the generalised dispersion model of Gill and Sankarasubramanian (1970) is used to study the axial dispersion in a Bingham fluid bound by permeable porous walls in the presence of electric and magnetic fields. MATHEMATICA 12.0 is used to calculate the most prominent dispersion coefficient, which is then graphically shown for various values of the Hartmann number (M=1,1.1,1.2,1.3), electric number (We=5,15,25,35), rheological parameter ($\eta_c = 0,0.1,0.15,0.2$) and porous parameter σ=(10,60,100,120).

Figures 2-5 elucidate the results of Eq. (26), when used to calculate the velocity with η, as well as the various impacts of the Hartmann and electric numbers, and the rheological parameter and porous parameters. Figures 2, 4, and 5 show that blood flow decreases in synovial fluid as the Hartmann number (Ha), rheological parameter (η_c), and porosity parameter(σ) rise. Increased magnetic, viscous, and resistive forces that obstruct fluid dynamics are the cause of this phenomena. According to studies, increasing Ha, η_c, and σ causes the fluid velocity to drop, the thickness of the boundary layer to grow, and the mixing to decrease Tripathi and Kumar (2020), Singh and Kumar(2020). This consequently enables decreased blood flow and nourishment supply to the joint tissues. Figure 3 illustrates that a rise in the electric number causes the blood flow to increase and also the velocity profile is parabolic. The electrokinetic effects, which improve fluid dynamics and mass transfer, are responsible for this occurrence. According to studies, a higher electric number causes the fluid velocity to increase, the thickness of the boundary layer to decrease, and mixing to improve. Increased blood flow and the transportation of nutrients to the joint tissues are so made possible.

Figure 6 show that the dispersion coefficient, computed for different values of the Hartmann number with dimensionless time . From this figure, we observe that the increase in Hartmann number, the axial dispersion coefficient increases. Figure 7-9 shows that dispersion coefficient increases with an increase in electric number, porosity parameter(σ) and rheological parameter (η_c). This result is useful in understanding one of the causes for haemolysis which in turn is useful in the design of an artificial organ. We have compared the calculated results for the dispersion coefficient with those of a past research of comparable problem for the flow of couple stress fluid in order to validate the results of the current investigation. It may be noted that the small differences may be attributed to be due to the fact that the fluid model of the present study is different from that used Mallika and Rudraiah (2011).

Figures 10 to 13 depicts the mean concentration θ_m with τ for different values of M, We and σ and η_c, inside the slug. From Figure 10, we observe that θ_m increases with increasing electric number, porosity parameter(σ) and rheological parameter (η_c). Figure 14-16 shows that increasing value of electric number, porosity parameter(σ) and rheological parameter (η_c) decrease θ_m. When the length of the initial slug input is increased from $\xi_s = 0.019$ to $\xi_s = 0.5$ the concentration decrease inside the slug and increase outside the slug. This is graphically represented in figure 18. The above results are useful in the control of haemolysis.

The transport of major metabolizes (such as sugar and aminoacids) is rather slow and convective transport plays a major role in accelerating them. Therefore, we have studied the mean concentration distribution θ_m with axial distance ξ for different values of M which are represented graphically in figures 14. The effects of increasing M, increases θ_m for $\xi_s = 0.019$, τ=0.06. Figure 15-17 depicts that the θ_m versus ξ for different value of electric number, porosity parameter(σ) and rheological parameter (η_c), it shows that θ_m decrease with an increase in electric number, porosity parameter(σ) and rheological parameter (η_c), for very small values of τ,concentration of blood shows a rapid increase.

5. CONCLUSION

This study presents a comprehensive analytical model to investigate the behavior of synovial fluid under the influence of electromagnetic fields and porous medium constraints. The use of a Bingham fluid model and the application of a generalized dispersion framework provide a physiologically relevant representation of solute transport in joint tissues. Importantly, this model does more than illustrate mathematical elegance; it contributes to medical science by offering insights into the dynamics of nutrient distribution and blood flow within joint cavities. The parametric analysis shows how key biomedical parameters, such as Hartmann number, electric number, rheological factors, and porosity, affect both the velocity profile and the dispersion of solutes. These findings carry direct implications for the design of prosthetic joints, optimization of therapeutic drug delivery, and reduction of haemolytic effects in artificial implants. The inclusion of realistic boundary conditions and medical relevance ensures that the model is both mathematically rigorous and clinically applicable. By linking advanced mathematical theory with practical biomedical goals, this work contributes to the growing interdisciplinary field of biomathematics and offers a foundation for future experimental validations and technological innovations in biomedical engineering.

REFERENCES

Alshehri, M. and Sharma, S.K., Computational Model for the Generalized Dispersion of Synovial Fluid, *Int. J. Adv. Comput. Sci. Appl.*, vol. **8**, no.2, pp.134–138, 2017. DOI: 10.14569/IJACSA.2017.080218

Beavers, G.S. and Joseph D.D., Boundary Conditions at a Naturally Permeable Wall, *J. Fluid Mech.,* vol. **30**, no.1, pp. 197-207,1967. DOI:10.11017/S002211206 7001375

Bég, O.A. and Roy, A.K., Moment Analysis of Unsteady Bi-Component Species (Drug) Transport with Coupled Chemical Reaction in Non-Newtonian Blood Flow, *Chinese Journal of Physics*, vol.**77**, pp. 1810–1826, 2022. DOI: 10.1016/j.cjph.2022.04.003

Christopherson, D.C. and Dowson, D., An Example of Minimum Energy Dissipation in Viscous Flow, *Proceedings of the Royal Society of London. Series A*, *Mathematical and Physical Sciences*, vol. **251**, no. 1267, pp. 550-564, 1959. DOI: 10.1098/rspa.1959.0128

Das, P., Sarifuddin, S., Rana, J. and Mandal, P.K., Solute Dispersion in Transient Casson Fluid Flow through Stenotic Tube with Exchange Between Phases, *Phys.Fluids*, vol. **33**, no. 6, 2021. DOI:10.1063/5.0052770.

Gill, W.N. and Sankarasubramanian, R., Exact Analysis of Unsteady Convective Diffusion, *Proceedings of the Royal Society of London. Series A,* Mathematical and Physical Sciences, vol. **316**, no. 1526, pp.341-350, 1970. DOI:10.1098/rspa.1970.0083

Jyoti, Kwak, S., Ham, S. and Kim, J., Dispersion and Phase Exchange Process of Chemically Reactive Solute through Circular Tube, *Journal of Applied Fluid Mechanics*, vol. **17**, no. 4, pp. 726-741, 2024. DOI:10.47176/jafm.17.4.2305

Le, A.D. and Tran, H.T., Improvement of Mass Transfer Rate Modeling for Prediction of

Cavitating Flow, *Journal of Applied Fluid Mechanics*, vol.**15**, no.2, pp. 551-561,2022. DOI: 10.47176/jafm.15.02.33231.

Mallika, K.S. and Rudraiah, N., Generalized Dispersion of Unsteady Convective Diffusion ni Couple Stress Poorly Conducting Fluid Bounded by Porous Layer in the Presence of an Electric Field, *World Journal of Engineering*, vol. **8**, no.4, pp. 335-346, 2011. DOI: 10.1260/1708-5284 .8.4.335.

Misra, J.C. and Adhikary, S.D., Flow of a Bingham Fluid in a Porous Bed under the Action of a Magnetic Field: Application to Magneto-Hemorheology, *Engineering Science and Technology, an International Journal*, vol. **20**, no. 3, pp.973–981, 2017, DOI: 10.1016/j.jestch.2016.11.008

Mohseni, M. and Domfeh, M.K., Numerical Analysis of Transient Vortex Formation at the Outlet of a Tank Containing Gas-Liquid Phases*, Journal of Applied Fluid Mechanics*, vol. **16**, no. 11, pp. 2235–2248, 2023. DOI:10.47176/jafm.16.11.1942

Nihaal, K.M., Mahalbaleshwar, U.S., Zeidan, D., and Woo Joo, S., Impact of Quadratic Thermal Radiation on MHD Nanofluid Flow across a Stretching Sheet with Variable Thickness: Xue and Yamado-Ota Thermophysical Model, *Acta Mechanica Sinica*, vol. **41**, no. 6, 2025. DOI:10.1007/s10409-024-24405-x.

Ratchagar, N. and Kumar, R., Effect of Couple Stress and Magnetic Field on the Unsteady Convective Diffusion in Blood Flow, *World Journal of Engineering*, vol. **11**, no.4, pp. 403-412, 2014. DOI:10.1260/1708-5284.11.4.403

Rudraiah, N., Devaraju, N. and Chiu-On, N.G., Electrohydrodynamic Dispersion on Deformable Aerosols in the Presence of an Electric Field and Chemical Reaction Using Taylor Dispersion Model, *Journal of Hydrodynamics, Ser.B* , vol. **23**, no. 2, pp. 247-257, 2011.

DOI:10.1016/S1001-6058(10)60110-2

Rushi Kumar, B., Vijayakumar, R. and Jancy Rani, A., A Model for the Generalised Dispersion of Synovial Fluids on Nutritional Transport with Joint Impacts of Electric and Magnetic Field, *Math. Comput.Appl.,* vol. **28**, no. 1, 2023.DOI: 10.3390/mca28010003

Sankara R., Introduction to Partial Differential Equations, 3rd ed., *Prentice Hall of India,* 1995.

Shaw, S., Ganguly, S., Sibanda, P. and Chakraborty, S., Dispersion Characteristics of Blood During Nanoparticle Assisted Drug Delivery Process through a Permeable Microvessel, *Microvascular Research*, vol. **92**, pp.25–33. DOI:10.1016/j.mvr.2013.12.007

Singh, J. and Kumar, V., Numerical Study of Electric Field Effects on Synovial Fluid Dynamics, *Journal of Biomechanics*, vol. **98**, 109433, 2020.

Taylor, G.I., Dispersion of Soluble Matter in Solvent Flowing Slowly through a Tube, *Proc. Roy., Soc. London*. 219, pp.186-203, 1953.DOI: 10.1098/rspa.1953.0139

Tandon, P.N., Nirmala, P., Pal, T.S. and Agarwal, R., Rheological Study of Lubricant Gelling in Synovial Joints during Articulation, *Appl. Math. Model,* vol. **12**, pp. 72–77, 1988.

Tripathi, D. and Kumar, V., Electrokinetic Effects on Blood Flow through a Narrow Channel, *Journal of Fluids Engineering*, vol. **142**, no. 10,pp. 101202, 2020.

APPENDIX A.

$$A_1 = \frac{s_5 + s_4 A_2}{s_3}, A_2 = \frac{s_5 s_4 - s_6 s_3}{s_3^2 - s_4^2}, A_3 = 0, A_4 = \frac{-s_7}{6}, A_5 = \frac{A_2 - A_1}{M} CoshM - \frac{We\, s_1 \alpha}{2M^2},$$

$$A_6 = -\frac{(A_2 + A_1)}{M^3} SinhM + \frac{We\, s_1}{6M^2},$$

$$s_1 = \frac{X_0 \alpha_c Pe}{2}, s_2 = \frac{\mathrm{Re}}{Pe}\frac{\partial p}{\partial \xi}$$

$$s_3 = (M + \alpha\sigma)e^{M}$$

$$s_4 = (M - \alpha\sigma)e^{-M}$$

$$s_5 = \frac{We\, s_1}{M^2}\left(\alpha\sigma(1-\alpha_c) - \alpha_c\right) + \alpha\sigma U_{p1},$$

$$s_6 = \frac{We\, s_1}{M^2}\left(-\alpha\sigma(1+\alpha_c) - \alpha_c\right) - \alpha\sigma U_{p2},$$

$$U_{p1} = -\frac{1}{\sigma^2 + M^2}\left(\frac{\mathrm{Re}}{Pe} + We\, s_1(1-\alpha_c)\right), U_{p2} = -\frac{1}{\sigma^2 + M^2}\left(\frac{\mathrm{Re}}{Pe} + We\, s_1(1+\alpha_c)\right)$$

FIG. 1: Physical problem

FIG. 2: Effects of M on velocity profile

FIG. 3: Effects of We on velocity profile

FIG. 4: Effects of σ on velocity profile

FIG. 5: Effects of η_c on velocity profile

FIG. 6: Effects of M on on dispersion coefficient

FIG. 7: Effects of We on dispersion coefficient

FIG. 8: Effects of σ on dispersion coefficient

FIG. 9: Effects of η_c on dispersion coefficient

FIG. 10: Effects of M on mean concentration with τ

FIG. 11: Effects of We on mean concentration with τ

FIG. 12: Effects of σ on mean concentration with τ

FIG. 13: Effects of η_c on mean concentration with τ

FIG. 14: Effects of M on mean concentration with ξ

FIG. 15: Effects of We on mean concentration with ξ

FIG. 16: Effects of σ on mean concentration with ξ

FIG. 17: Effects of η_c on mean concentration with ξ

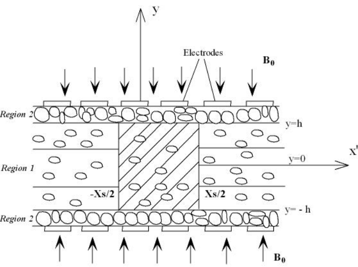
y
Electrodes
B_0
Region 2
y=h
X'
y=0
Region 1
-Xs/2
Xs/2
y= - h
Region 2
B_0

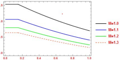

1.5
1.0
0.5
0.0
0.0
0.2
0.4
0.6
0.8
1.0
η
M=1.0
M=1.1
M=1.2
M=1.3

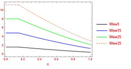

We=5
We=15
We=25
We=35

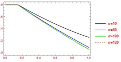
σ=10
σ=60
σ=100
σ=120
0.0
0.2
0.4
0.6
0.8
1.0
η

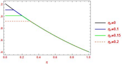
1.2
1.0
0.8
0.6
0.4
0.0
0.2
0.4
0.6
0.8
1.0
η
ηc=0
ηc=0.1
ηc=0.15
ηc=0.2

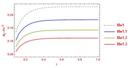

0.20
0.15
0.10
0.05
0.2
0.4
0.6
0.8
1.0
τ
M=1
M=1.1
M=1.2
M=1.3

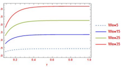

$\kappa_2 \cdot Pe^{-2}$
r
We=5
We=15
We=25
We=35

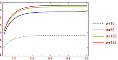

0.40
0.35
0.30
0.25
0.20
0.15
0.10
0.05
0.2
0.4
0.6
0.8
1.0
r
σ=10
σ=60
σ=100
σ=120

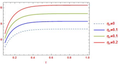
0.20
0.15
0.10
0.2
0.4
0.6
0.8
1.0
T
η_c=0
η_c=0.1
η_c=0.15
η_c=0.2

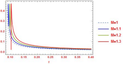

0.4
0.3
0.2
0.1
0.0
0.10
0.15
0.20
0.25
0.30
0.35
0.40
T
M=1
M=1.1
M=1.2
M=1.3

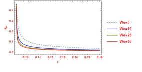

We=5
We=15
We=25
We=35
0.4
0.3
0.2
0.1
0.0
0.10
0.11
0.12
0.13
0.14
0.15
0.16
r

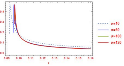

0.4
0.3
0.2
0.1
0.0
0.09
0.10
0.11
0.12
0.13
0.14
0.15
0.16
r
σ=10
σ=60
σ=100
σ=120

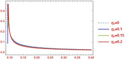

η_H
0.0
0.1
0.2
0.3
0.4
0.10
0.15
0.20
0.25
0.30
0.35
0.40
r
η_c=0
η_c=0.1
η_c=0.15
η_c=0.2

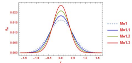

θ_m
0.020
0.015
0.010
0.005
0.000
-1.5
-1.0
-0.5
0.0
0.5
1.0
1.5
ξ
M=1
M=1.1
M=1.2
M=1.3

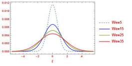

0.012
0.010
0.008
0.006
0.004
0.002
0.000
-4
-2
0
2
4
ξ
We=5
We=15
We=25
We=35

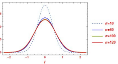

0.015
0.010
0.005
0.000
θ_{rr}
−2
−1
0
1
2
ζ
σ=10
σ=60
σ=100
σ=120

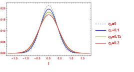

θm
0.020
0.015
0.010
0.005
0.000
-1.5
-1.0
-0.5
0.0
0.5
1.0
1.5
ζ
ηc=0
ηc=0.1
ηc=0.15
ηc=0.2